Exploring s-d, s-f, and d-f Electron Interactions in Ag_nCe^+ and Ag_nSm^+ by Chemical Reaction toward O_2

Arakawa, Masashi
Department of Chemistry, Faculty of Science, Kyushu University

Hayashi, Naho
Department of Chemistry, Faculty of Science, Kyushu University

Minamikawa, Kento
Department of Chemistry, Faculty of Science, Kyushu University

Nishizato, Tasuku
Department of Chemistry, Faculty of Science, Kyushu University

他

出版情報：The Journal of Physical Chemistry A. 126 (39), pp.6920-6926, 2022-09-26. American Chemical Society (ACS)
バージョン：

Exploring s–d, s–f, and d–f Electron Interactions in Ag_nCe^+ and Ag_nSm^+ by Chemical Reaction toward O_2

Masashi Arakawa, Naho Hayashi, Kento Minamikawa, Tasuku Nishizato, and Akira Terasaki**

Department of Chemistry, Faculty of Science, Kyushu University, 744 Motooka, Nishi-ku, Fukuoka 819-0395, Japan

ABSTRACT

We investigate gas-phase reactions of free Ag_nCe^+ and Ag_nSm^+ clusters with oxygen molecules to explore s−d, s−f, and d–f electron interactions in the finite size regime; a Ce atom has a 5d electron as well as a 4f electron, whereas a Sm atom has six 4f electrons without 5d electrons. In the reaction of Ag_nCe^+ (n = 3–20), the Ce atom located on the cluster surface provides an active site except for n = 15 and 16, as inferred from the composition of reaction products with oxygen bound to the Ce atom as well as from their relatively high reactivity. The extremely low reactivity for n = 15 and 16 is due to encapsulation of the Ce atom by Ag atoms. The minimum reactivity observed at n = 16 suggests that a closed electronic shell with 18 valence electrons is formed with a delocalized Ce 5d electron, while the localized Ce 4f electron does not contribute to the shell closure. As for Ag_nSm^+ (n = 1–18), encapsulation of the Sm atom was observed for $n \geq 15$. The lower reactivity at n = 17 than at n = 16 and 18 implies that an 18-valence-electron shell closure is formed with s electrons from Ag and Sm atoms; Sm 4f electrons are not involved in the shell closure as in the case of Ag_nCe^+. The present results suggest that the 4f electrons tend to localize on the lanthanoid atom, whereas the 5d electron delocalizes to contribute to the electron shell closure.

1. INTRODUCTION

Electronic properties of dilute magnetic alloys are characterized by interaction between itinerant s electrons from a host metal and d electrons from a magnetic impurity atom, as is known as the Kondo effect.[1] The magnitude of s–d interaction depends on the combination of impurity and host metal atoms; the magnetic moment vanishes if the s–d interaction is strong.[2,3] As for magnetic alloys containing a lanthanoid element as an impurity, the heavy-fermion state[4] emerges as a result of competition between the Kondo effect, which reduces the magnetic moment by hybridization of conduction electrons with f electrons, and the Ruderman–Kittel–Kasuya–Yosida (RKKY) interaction,[5–7] which encourages magnetic ordering. Heavy-fermion systems that exhibit a low-temperature resistivity rise, e.g., SmB_6,[8] $Ce_3Bi_4Pt_3$,[9] and $CeOs_2Al_{10}$,[10] are known as Kondo insulators.

When the size of the alloy is reduced to nanoscale, s–d, s–f, and d–f interactions are not trivial because itinerant electrons occupy discrete energy levels instead of the band structure in a bulk metal. As for s–d interaction, a variety of doped metal clusters, especially, group 11 metal clusters doped with a d-block transition-metal atom, have been investigated both by experiment and by theory. Theoretical studies revealed that group 11 metal clusters with an icosahedral geometry enclosing a group 6 dopant, e.g., $Au_{12}W$,[11] $Ag_{12}Mo$,[12,13] $Ag_{12}W$,[12] and $Cu_{12}Cr$,[14] form a closed-electronic shell with 18 electrons including delocalized d electrons from the dopant: for example, 12 Au $6s^1$ and W $5d^4$ $6s^2$ for $Au_{12}W$.[11] These species exhibit notable features in their properties, e.g., a high binding energy and a large HOMO–LUMO gap. By further theoretical studies on 3d-transition-metal doped Ag and Cu clusters, $Ag_{15}Sc$,[15] $Ag_{14}Ti$,[16] $Cu_{14}V^+$,[17] $Ag_{14}V^+$,[17,18] Ag_9Co,[19,20] and $Ag_{10}Co^+$,[20] were found to be 18-electron stable species with large HOMO–LUMO gaps.

The first experimental report of such doped clusters was on free 3d-transition-metal-doped Au cluster cations, Au_NM^+ (M = Sc–Ni), where abundance of the cluster cations was measured after photofragmentation to identify stable sizes *N*.[21,22] Formation of an 18-electron closed shell was manifested by prominent abundance of $Au_{16}Sc^+$ and $Au_{15}Ti^+$, which consist of delocalized 4s and 3d electrons of Sc $3d^1\ 4s^2$ and Ti $3d^2\ 4s^2$, Au $6s^1$ from each Au atom, and minus one for the positive charge, whereas only 4s electrons were found to delocalize for other dopants (Cr, Mn, Fe, Co, and Ni). The experiment was extended to Ag clusters doped with a 3d transition-metal atom, Ag_NM^+,[23,24] and Cu clusters doped with a Sc atom, Cu_NSc^+,[25,26] where $Ag_{16}Sc^+$, $Ag_{15}Ti^+$, $Ag_{14}V^+$, $Ag_{11}Fe^+$, $Ag_{10}Co^+$, Ag_9Ni^+, and $Cu_{16}Sc^+$ were identified as stable clusters, suggesting 18-electron shell closures with delocalized 3d electrons. It was revealed indeed for $Ag_{10}Co^+$ by DFT calculation that 1S-, 1P-, and 1D-like superatomic orbitals are occupied by Ag 5s and delocalized Co 4s and 3d electrons, resulting in a singlet state with completely unpolarized spins, and, therefore, that the magnetic moment on the dopant Co is quenched.[23] In addition to these photofragmentation studies, X-ray magnetic circular dichroism (XMCD) spectroscopy has been carried out, where the local magnetic moment on the dopant Cr atom in Au_NCr^+ (N = 2–7) is reported to correlate with the energy gap of the host Au cluster, showing a finite-size effect in s–d interaction.[27]

In this context, we have reported systematic measurements of reactivity of the doped clusters against O_2; oxygen etching is frequently employed to examine stability of clusters.[28–30] By performing multiple-collision reaction experiments, not only the reactivity but also successive elementary reaction processes can be revealed.[31–41] We have found that the doped anionic clusters, $Ag_{14}Sc^-$, $Ag_{13}Ti^-$, and $Ag_{12}V^-$, as well as cationic clusters, $Ag_{16}Sc^+$, $Ag_{15}Ti^+$, $Ag_{14}V^+$, $Ag_{11}Fe^+$, $Ag_{10}Co^+$, and Ag_9Ni^+, exhibit a

reactivity minimum in the size-dependent measurement of reaction rate coefficients along with reaction kinetics;[42–45] the low reactivity suggests that these clusters are stable due to the 18-electron shell closure including delocalized 3d electrons of the dopant atom. In contrast, Ag_9Fe^-, Ag_8Co^-, and Ag_7Ni^-, possessing an exohedral dopant geometry, were highly reactive even with 18 valence electrons, which suggests that an endohedral geometry plays a key role in 3d delocalization.[45]

In contrast to the numerous studies on s–d interactions, s–f and d–f interactions have not been reported in nanoscale doped clusters. Behavior of 4f electrons in lanthanoids cannot be predicted from the studies of s–d interaction because they are highly screened by 5s and 5p electrons. In the present study, we investigate reaction of cerium- and samarium-doped silver cluster cations, Ag_nCe^+ and Ag_nSm^+, with O_2 molecules to examine their size-dependent reactivity and thus to clarify whether 5d and 4f electrons participate in the electronic-shell closure formed by 18 electrons; Ce ([Xe] $4f^1\ 5d^1\ 6s^2$) with a 5d electron as well as a 4f electron and Sm ([Xe] $4f^6\ 6s^2$) without a 5d electron were selected as dopants.

2. METHODS

The experimental apparatus and procedures have been described in detail elsewhere.[43] Briefly, Ag_nCe^+ (n = 3–20) and Ag_nSm^+ (n = 1–18) were produced by a magnetron-sputtering cluster-ion source,[46] where two metal-target plates were cosputtered by placing a cerium plate (Kojundo Chemical Laboratory, 99.9%) or a samarium plate (Kojundo Chemical Laboratory, 99.9%) under a silver plate (Toshima Manufacturing, 99.99%) with two 8-mm holes. The size and the number of the holes were adjusted to produce relatively large clusters efficiently. The produced cluster cations were size-selected by a

quadrupole mass filter (MAX-4000, Extrel CMS) after thermalization by collisions with a He gas cooled by liquid N_2. The size-selected reactant cluster cations guided by home-made radio-frequency (rf) octopole ion guides and quadrupole deflectors were loaded into a 30-cm-long linear quadrupole ion trap for 50–200 ms at a translational energy of ~10 eV in the laboratory frame. The ion trap was placed in a reaction gas cell, which was filled with a reactant O_2 gas and a buffer He gas at room temperature. The partial pressure of the He gas was adjusted at 0.3 Pa, whereas that of O_2, P_{O2}, was controlled in the range from 5×10^{-5} to 3×10^{-2} Pa depending on the magnitude of reactivity so that the reaction rate constant came into the time window of the measurement. A residual gas analyzer (RGA100, Stanford Research Systems) was used to measure the pressures outside the reaction cell, which were converted to the pressures inside the cell as reported previously[31] by referring to the reaction cross sections known for Co_N^+ against O_2.[47] Reactant cluster cations admitted into the ion trap were stored for a variable time, t, for reaction. Ions produced through the reaction were extracted from the ion trap, and were analyzed by a reflectron time-of-flight (TOF) mass spectrometer improved by our own techniques.[48,49] The TOF signals from a micro-channel-plate (MCP) detector (F4655-14, Hamamatsu Photonics) were acquired by an oscilloscope (HDO4054, Teledyne LeCroy, 500 MHz) through a preamplifier (SR445A, Stanford Research Systems). The yields of ions of the reactant and products were recorded as a function of storage time t to analyze reaction kinetics.

3. RESULTS

3.1 Reaction products. *3.1.1. Ag_nCe^+.* Figure 1 shows time-of-flight mass spectra of product ions upon reaction of Ag_nCe^+ with O_2 molecules for n = 3–20. The

major reaction products for $n \leq 12$ are $Ag_{n'}^+$ with odd n' ($n' < n$). For example, as shown in Fig. 1h, Ag_9^+ is produced from $Ag_{10}Ce^+$, which would be associated with a release of neutral $AgCeO_2$. In addition to $Ag_{n'}^+$, $Ag_{n''}CeO_2^+$ ($n'' < n$) is observed for $n \leq 7$. For example, $Ag_3CeO_2^+$ as well as Ag_3^+ and Ag_5^+ are observed as the major products for n = 7 as shown in Fig. 1e. As for $n \geq 13$, except for n = 15 and 16 with extremely low reactivity, production of Ag_n^+ is the major reaction channel, which is associated with a release of neutral CeO_2. It should be noted that O_2 seems to be always bound to the Ce atom after reaction except for n = 15 and 16.

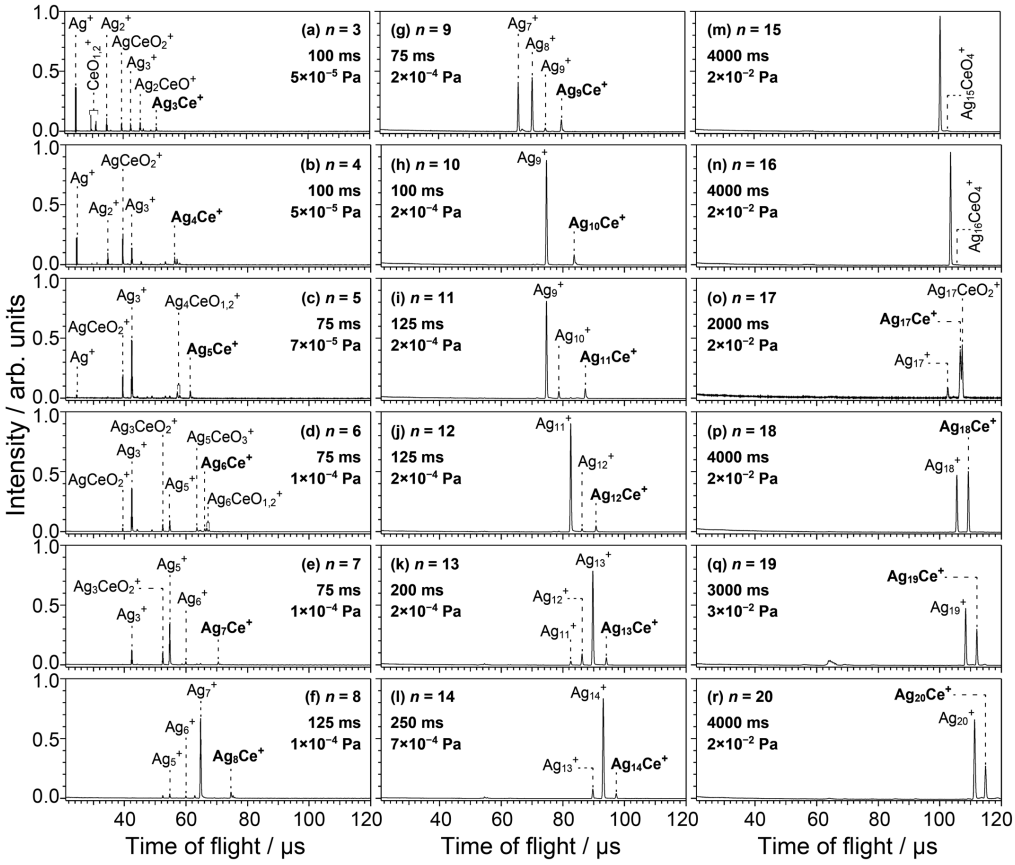

Figure 1. Time-of-flight mass spectra of ions produced from the reaction of Ag_nCe^+ with O_2 for n = 3–20 in panels a–r, respectively. The storage time, t, and the partial pressure of O_2, P_{O2}, are given in each panel.

3.1.2. Ag_nSm^+. The time-of-flight mass spectra of product ions for Ag_nSm^+ are shown in Fig. 2 for n = 1–18. The major reaction products for $4 \le n \le 13$ are $Ag_{n'}SmO_m^+$ with even n' ($n' < n$). For example, $Ag_4SmO_{2-4}^+$ and $Ag_6SmO_{2-4}^+$ are the major reaction products for n = 8 as shown in Fig. 2h. For n = 2 and 3, $AgSmO_m^+$ is the major reaction product. In addition to these products, Ag^+ is observed for n = 1 and 2, and Ag_3^+ is observed for n = 5 and 6. As for $n \ge 14$, formation of O adducts without dissociation, $Ag_nSmO_m^+$, is the major reaction channel, e.g., $Ag_{16}SmO_4^+$ for n = 16 as shown in Fig. 2p, although the reactivity is very low.

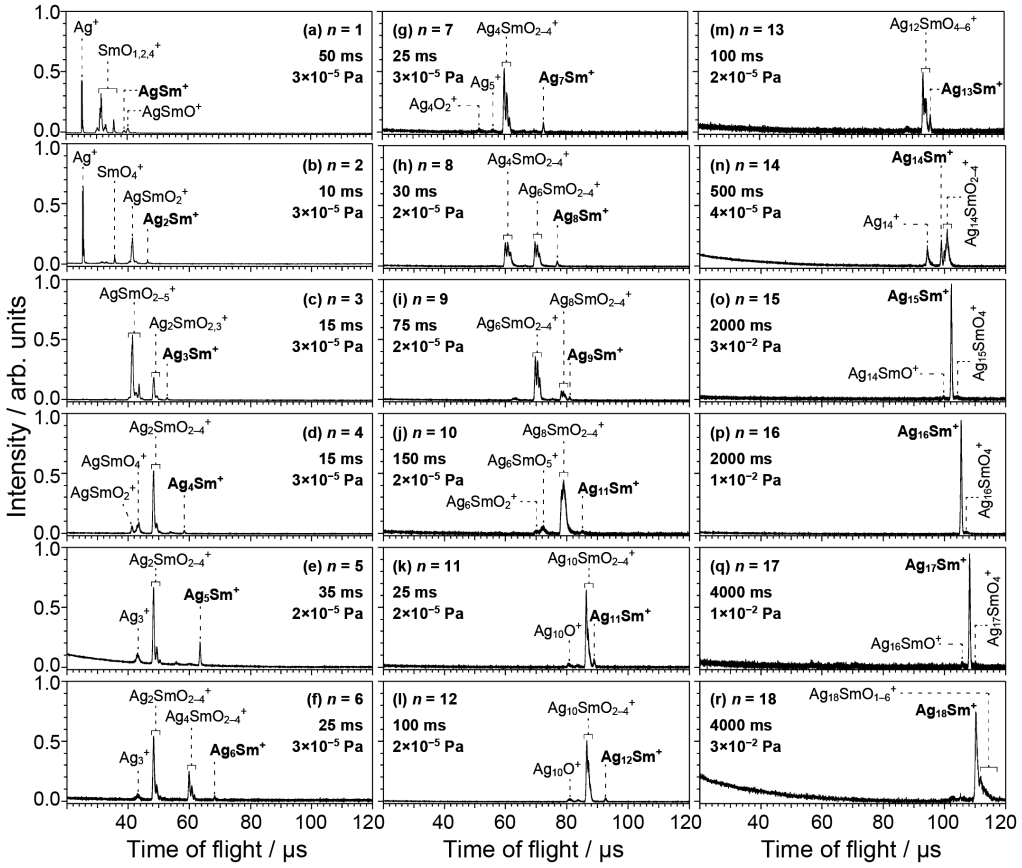

Figure 2. Time-of-flight mass spectra of ions produced from the reaction of Ag_nSm^+ with O_2 for n = 1–18 in panels a–r, respectively. The storage time, t, and the partial pressure of O_2, P_{O2}, are given in each panel.

3.2 Reactivity evaluated by an extinction rate of the reactant. Time-dependent measurements were performed to evaluate the depletion rate constant of the reactants, Ag_nCe^+ and Ag_nSm^+, which was divided by oxygen concentration to obtain a reaction rate coefficient in the same way as reported for 3d-transition-metal-doped clusters.[43] The reaction rate coefficients thus obtained for Ag_nCe^+ and Ag_nSm^+ are shown in Fig. 3a and 3b, respectively, along with those of undoped Ag_n^+. These rate coefficients are relative to that of Ag_8^+, $(6 \pm 2) \times 10^{-15}$ cm^3 s^{-1},[39,43] so that they can be compared with those of $Ag_n^{+/-}$ and $Ag_nM^{+/-}$ (M = Sc–Ni) reacting with O_2 and NO reported previously.[39,41,43–45] Note that the absolute values of reaction rate coefficients suffer from a systematic error as high as 30% mainly due to uncertainty in the O_2 pressure in the ion trap measured in a manner described in Section 2; the relative values displayed in Fig. 3 show the size dependence clearly, which are subject only to a statistical error of about 5%.

The reaction rate coefficient of Ag_nCe^+ was more than 4 orders of magnitude higher than that of Ag_n^+ for $n \leq 13$; the presence of a Ce atom strongly enhances the reactivity. It gradually decreases with the size, and then dramatically decrease from n = 14 to 15 as shown in Fig. 3a. It reaches a reactivity minimum at n = 16, and turns to increase for $n \geq 17$. The reactivity for $n \geq 17$ is larger than those of Ag_n^+. As for Ag_nSm^+ in Fig. 3b, the reactivity for $n \leq 13$ was more than 4 orders of magnitude higher than that of Ag_n^+, and it exhibits a decreasing trend with the size as in the case of Ag_nCe^+. It also dramatically decreases from n = 14 to 15. Fig. 3b shows that the reactivity of Ag_nSm^+ for n = 15–18 is comparable with those of Ag_n^+, which is in contrast to the case of Ag_nCe^+.

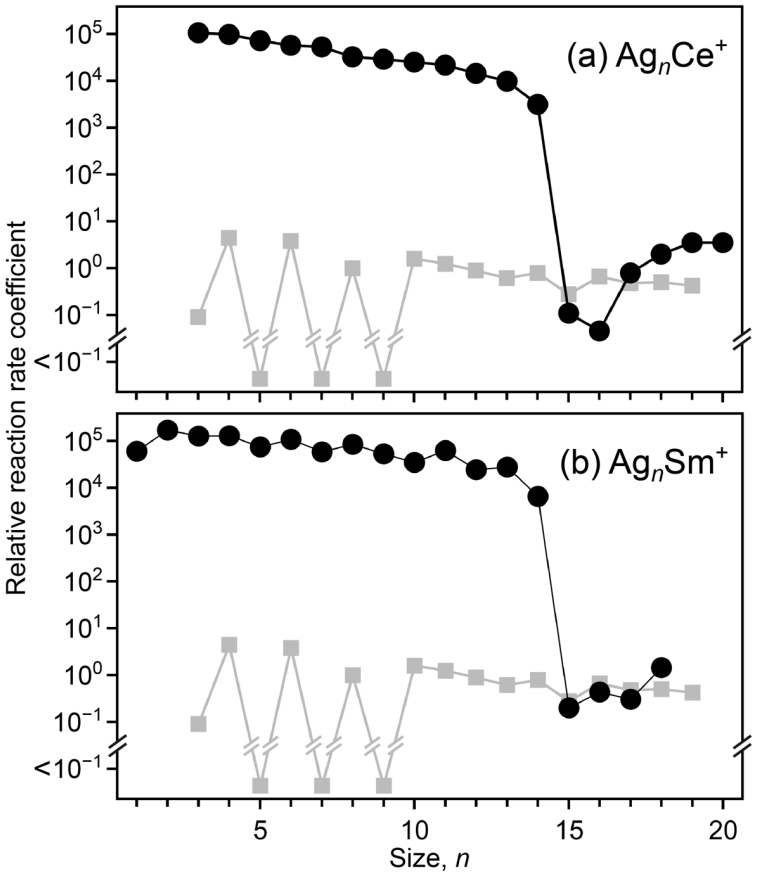

Figure 3. Size dependence of reaction rate coefficients of (a) Ag_nCe^+ and (b) Ag_nSm^+ toward O_2 along with undoped Ag_n^+ in gray. The values are relative to that of Ag_8^+, which is reported to be $(6 \pm 2) \times 10^{-15}$ cm^3 s^{-1};[39,43] statistical uncertainties in the relative values were so small that error bars are not discernible in the data points. The value $<10^{-1}$ indicates that no product was observed with the present sensitivity of ion detection.

4. DISCUSSION

4.1 Electronic and geometric structures of Ag_nCe^+. As described in Section 3, reaction rate coefficients of Ag_nCe^+ for $n \leq 14$ are much higher than that of Ag_n^+, which are very close to that reported previously for Ce^+.[50] In this size range, the major reaction products is $Ag_{n'}^+$ and $Ag_{n''}CeO_2^+$ for $n \leq 7$, and $Ag_{n'}^+$ for $8 \leq n \leq 13$, where n' and n'' are

odd numbers smaller than n. These ions are produced via an intermediate ion−molecule complex, $Ag_nCeO_2^+$, which is not discernible in the mass spectra. Dissociation of Ag atoms from the intermediate complex forms $Ag_{n''}CeO_2^+$, while dissociation of CeO_2 along with Ag atom(s) produces $Ag_{n'}^+$. The formation of neutral CeO_2 is attributed to its high ionization potential. The Ce atom located on the cluster surface provides an active site as inferred from the fact that the reactant oxygen is always bound to the Ce atom in the reaction products. In the reaction of Ce^+ with O_2, promotion of one electron from the ground-state valence configuration of Ce^+, $4f^15d^26s^0$, to $4f^15d^16s^1$ was reported to be a key process of the reaction; two unpaired electrons, $5d^16s^1$, are donated to the oxygen to make Ce^+−O bonding,[50] where the 4f electron does not participate in the reaction. Since the ionization potential of Ce is smaller than those of Ag and Ag clusters,[51] the positive charge of Ag_nCe^+ would be localized on the Ce atom to form Ce^+ essentially; it is speculated that the 5d electron of Ce^+ in Ag_nCe^+ is involved in the present reaction.

The gradual decrease in the rate coefficient with the size, as discernible in Fig. 3a, is probably due to that the active Ce site is gradually surrounded by Ag atoms, which leads to a sudden drop from n = 14 to 15. The low reactivity for n = 15 can be attributed to a fully encapsulated geometry of Ce, which reduces the adsorption energy of O_2 to the cluster because the reaction site changes from the Ce to a Ag atom. The lower adsorption energy would lead to lower reactivity and less fragmentation; in addition, the larger cluster would have a reduced rate of fragmentation due to its higher heat capacity.[38,52] A similar drop in reactivity upon encapsulation has been reported not only for doped Ag clusters[42,43,45] but also for doped Si and Cu clusters.[53−55] The reactivity drop for 3d-transition-metal-doped silver cluster cations, Ag_nM^+, occurred at $n \geq 14$, 12, 11, 10, 11, 11, 8, and 9 for M = Sc, Ti, V, Cr, Mn, Fe, Co, and Ni, respectively, as reported

previously.[43] The results imply that the encapsulation of Ce requires more Ag atoms than that for a 3d-transtion-metal atom due to the large atomic radius of Ce.

The encapsulation of the dopant atom is also manifested in the reaction products. Oxygen is always bound to the Ce atom in the reaction products for $n \leq 14$, suggesting that the Ce atom located on the cluster surface provides an active site. The large adsorption energy of O_2 on the Ce site induces dissociation of CeO_2 and Ag atom(s). On the other hand, the only reaction channel observed for $n = 15$ and 16 was formation of a trace amount of O adducts free from dissociation, which suggests that oxygen is bound very weakly to Ag atoms that completely encapsulate the Ce atom.

It is interesting that, although the Ce atom is once fully encapsulated at $n = 15$ and 16, it is again exposed on the cluster surface for $n \geq 17$. The major reaction product for $n = 17-20$ is Ag_n^+, which is associated with a release of CeO_2 without dissociation of Ag atoms. The dissociation of CeO_2 suggests that the Ce atom is not fully encapsulated by Ag atoms and provides an active site. The size $n = 17$ is a notable size, where both Ag_{17}^+ and $Ag_{17}CeO_2^+$ are observed as reaction products. Figure 4 shows temporal evolution of ion signals of the reactant and products as a function of storage time, t, for $Ag_{17}Ce^+$. The ion signal is defined as a fraction of each ion in the entire ions observed. Note that product ions were observed already at $t = 0$, which were produced during ion loading to the ion trap. The reactant $Ag_{17}Ce^+$ decreases exponentially with t in the initial stage, which almost levels off after 0.5 s. Accordingly, an oxygen adduct, $Ag_{17}CeO_2^+$, is formed as a product ion, which is slowly followed by formation of Ag_{17}^+. The result suggests that Ag_{17}^+ is produced via $Ag_{17}CeO_2^+$, while $Ag_{17}Ce^+$ and $Ag_{17}CeO_2^+$ reach almost equilibrium.

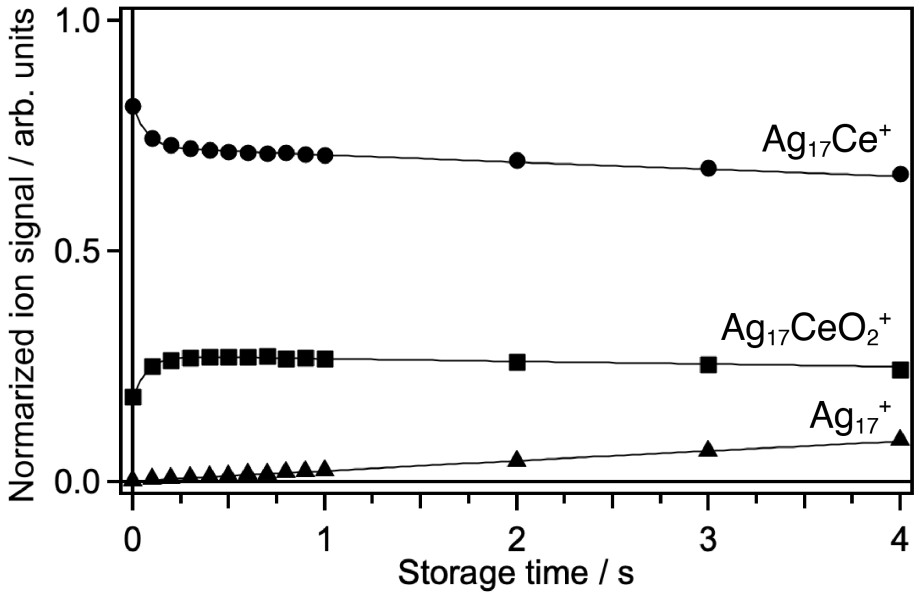

Figure 4. Reaction kinetics of $Ag_{17}Ce^+$ interacting with O_2 under $P_{O2} = 2 \times 10^{-2}$ Pa: $Ag_{17}Ce^+$ (closed circles), $Ag_{17}CeO_2^+$ (closed squares), and Ag_{17}^+ (closed triangles). The ion signals are normalized so that the total signal of the entire ions is unity at each storage time. Fitting curves are superimposed by solid lines.

The present reactions take place in a pseudo-first-order process because the partial pressures of O_2 and He gases in the reaction cell were kept constant much higher than the corresponding density of the reactant ions, $Ag_{17}Ce^+$. For analysis of reaction pathways, the kinetics data were fitted to rate equations by a program coded by referring to the DETMECH software[56] in the same way as we reported for the reaction of Ag_n^+ with NO.[39] The solid lines in Fig. 4 show data fitting to the following rate equations based on the reaction pathway shown in Scheme 1, which best reproduced the experimental data:

$$d[Ag_{17}Ce^+]/dt = -k_1[Ag_{17}Ce^+] + k_2[Ag_{17}CeO_2^+] \quad (1)$$

$$d[Ag_{17}CeO_2^+]/dt = k_1[Ag_{17}Ce^+] - (k_2 + k_3)[Ag_{17}CeO_2^+] \quad (2)$$

$$d[Ag_{17}^+]/dt = k_3[Ag_{17}CeO_2^+] \quad (3)$$

The pseudo-first-order rate constants of each step of the elementary reactions, k_1, k_2, and k_3 were obtained to be 3.77, 9.94, and 0.08 s^{-1}, respectively, at $P_{O2} = 2 \times 10^{-2}$ Pa. Note that the rate constant of O_2 dissociation from $Ag_{17}CeO_2^+$, k_2, is much larger than k_3. This is probably because an adsorption energy of O_2 on $Ag_{17}Ce^+$ is very low due to an almost encapsulated geometry of Ce.

$$Ag_{17}Ce^+ \underset{k_2}{\overset{k_1}{\rightleftharpoons}} Ag_{17}CeO_2^+ \xrightarrow{k_3} Ag_{17}^+$$

Scheme 1. Reaction pathways of $Ag_{17}Ce^+$ exposed to O_2 molecules. The parameters, k_1, k_2, and k_3, denote reaction rate constants of each step.

The analysis of reaction kinetics was also performed for n = 14 and 18 in the same way to show the specificity of n = 17. The reaction kinetics of n = 14 and 18 are shown in Figs. S1 and S2, respectively, of the Supporting Information. In each figure, solid curves show the best fit to pseudo-first-order rate equations based on the reaction pathways shown below the figure. The pseudo-first-order rate constants of each step of the reactions are given above each arrow in the unit of s^{-1}. For n = 14, the reactant, $Ag_{14}Ce^+$, decreases exponentially with the storage time and disappears almost completely within 0.5 s; Ag_{14}^+ is produced accordingly, which is followed by slow formation of Ag_{13}^+. As for n = 18, the reactant, $Ag_{18}Ce^+$, also shows an exponential decay, which is accompanied by formation of Ag_{18}^+ as a final product ion within 8 s. In both cases, an intermediate complex, $Ag_nCeO_2^+$, is not observed, which should be short-lived due to rapid fragmentation via a release of CeO_2. This behavior is in striking contrast to the case of n = 17, where $Ag_{17}Ce^+$ and $Ag_{17}CeO_2^+$ reach almost equilibrium. Furthermore,

reaction kinetics of n = 3 is presented in Fig. S3 of the Supporting Information as a representative of small sizes, which is rather complicated. Ag_2CeO^+ was found to be an intermediate for $AgCeO_2^+$, CeO^+, and CeO_2^+, while pure silver cluster cations, Ag^+, Ag_2^+, and Ag_3^+, are produced concomitantly with Ag_2CeO^+ from the reactant, Ag_3Ce^+.

For the endohedral clusters, n = 15 and 16, the minimum reactivity was observed at n = 16 rather than at n = 15. The result suggests that a closed electronic shell with 18 valence electrons is formed by 16 Ag 5s and 3 Ce 5d and 6s electrons minus one for the positive charge, not including Ce 4f. The 4f electron is not involved in the shell closure, whereas the 5d electron delocalizes to contribute to the shell closure. This might be due to the highly localized nature of 4f electrons screened by the 5s and 5p orbitals. The 4f electron localized on the encapsulated Ce atom would not participate in the reaction.

4.2 Electronic and geometric structures of Ag_nSm^+. As in the case of Ag_nCe^+, reaction rate coefficients of Ag_nSm^+ with $n \leq 13$ are much higher than those of Ag_n^+, and are rather in the same order of magnitude as reported previously for Sm^+.[50] The result implies that the Sm atom located on the cluster surface provides an active site. Note that, in contrast to the significant odd−even alternation observed for Ag_n^+ at small sizes, it is not clear for Ag_nSm^+, which also supports that the Sm atom provides a reaction site. Since the ionization potential of Sm is smaller than that of Ag and Ag clusters,[51] the positive charge of Ag_nSm^+ would be localized on the Sm atom to form Sm^+ essentially. In the reaction of Sm^+ with O_2, promotion of one electron from the ground-state valence configuration of Sm^+, $4f^6 5d^0 6s^1$, to $4f^5 5d^1 6s^1$ has been reported to be a key process for the reaction; two unpaired electrons, $5d^1 6s^1$, are donated to the oxygen to form a Sm^+−O bond.[50] In contrast to the case of Ce^+, where the 4f electron is not involved in the reaction, a 4f electron of Sm^+ participates in the reaction via its promotion to 5d.

The reactivity dramatically decreases from n = 14 to 15; at the same time, the reaction products changed from fragmented $Ag_{n'}SmO_m^+$ with even n' to $Ag_nSmO_m^+$ free from dissociation of Ag atoms. The result suggests a change in the reaction site from the Sm atom to a Ag atom at n = 15; the former gives high reactivity due to a 5d electron promoted from 4f. The oxygen is bound weakly to Ag atoms that encapsulate the Sm atom for $n \geq 15$. The lower reactivity at n = 17 than at n = 16 and 18 is consistent with the highly localized nature of 4f electrons as discussed for Ag_nCe^+; a closed electronic shell with 18 valence electrons is formed by 17 Ag 5s and one 6s from the ground-state Sm^+ without six 4f electrons.

5. CONCLUSIONS

Gas-phase reactions of free Ag_nCe^+ and Ag_nSm^+ clusters with oxygen molecules were studied to investigate s−d, s−f, and d−f interactions in the finite size regime. In the reaction of Ag_nCe^+, the Ce atom located on the cluster surface provides an active site except for n = 15 and 16, as inferred from the relatively high reactivity and the fact that oxygen was bound to the Ce atom as revealed by the analysis of reaction products. The minimum reactivity observed at n = 16 rather than at n = 15 suggests that a closed electronic shell with 18 valence electrons is formed by Ag 5s, Ce 6s, and Ce 5d electrons, not including Ce 4f; the 4f electron is not involved in the shell closure, whereas the 5d electron delocalizes to contribute to the shell closure. The localized 4f electron of the encapsulated Ce atom does not participate in the reaction, hence the minimum reactivity at n = 16. As for Ag_nSm^+, encapsulation of the Sm atom was observed at n = 15. The lower reactivity at n = 17 than at n = 16 and 18 implies that a closed electronic shell with 18 valence electrons is formed by 17 Ag 5s and one 6s from Sm^+ without six 4f electrons.

The present results suggest a tendency for the 4f electrons to localize on a lanthanoid atom; the 5d electrons, in contrast, delocalize to contribute to the 18-electron shell closure.

ASSOCIATED CONTENT

Supporting Information

The Supporting Information is available free of charge on the ACS Publications website at DOI: xxx. Reaction kinetics of Ag_3Ce^+, $Ag_{14}Ce^+$, and $Ag_{18}Ce^+$ interacting with O_2; and a complete list of authors of Ref. 54. (PDF)

AUTHOR INFORMATION

Corresponding Authors

* (M.A.) E-mail: arakawa@chem.kyushu-univ.jp

* (A.T.) E-mail: terasaki@chem.kyushu-univ.jp

Notes

The authors declare no competing financial interest.

ACKNOWLEDGMENTS

The present study was supported by JSPS KAKENHI Grant Numbers JP18H03901, JP19K05185 and JP22H01288 and MEXT KAKENHI Grant Number JP17H06456.

REFERENCES

(1) Kondo, J. Resistance Minimum in Dilute Magnetic Alloys. *Prog. Theor. Phys.* **1964**, *32*, 37–49.

(2) Daybell, M. D.; Steyert, W. A. Localized Magnetic Impurity States in Metals: Some Experimental Relationships. *Rev. Mod. Phys.* **1968**, *40*, 380–389.

(3) Heeger, A. J. Localized Moments and Nonmoments in Metals: The Kondo Effect. *Solid State Phys.* **1970**, *23*, 283–411.

(4) Andres, K.; Graebner, J. E.; Ott, H. R. 4*f*-Virtual-Bound-State Formation in $CeAl_{13}$ at Low Temperatures. *Phys. Rev. Lett.* **1975**, *35*, 1779–1782.

(5) Ruderman, M. A.; Kittel, C. Indirect Exchange Coupling of Nuclear Magnetic Moments by Conduction Electrons. *Phys. Rev.* **1954**, *96*, 99–102.

(6) Kasuya, T. A Theory of Metallic Ferro- and Antiferromagnetism on Zener's Model. *Prog. Theor. Phys.* **1956**, *16*, 45–57.

(7) Yoshida, K. Magnetic Properties of Cu-Mn Alloys. *Phys. Rev.* **1957**, *106*, 893–898.

(8) Menth, A.; Buehler, E.; Gaballe, T. H. Magnetic and Semiconducting Properties of SmB_6. *Phys. Rev. B* **1968**, *88*, 180405.

(9) Hudley, M. F.; Canfield, P. C.; Thompson, J. D.; Fisk, Z. Hybridization Gap in $Ce_3Bi_4Pt_3$. *Phys. Rev. B.* **1990**, *42*, 6842–6845.

(10) Kimura, S.; Iizuka, T.; Miyazaki, H.; Irizawa, A.; Muro, Y.; Takabatake, T. Electronic-Structure-Driven Magnetic Ordering in a Kondo Semiconductor $CeOs_2Al_{10}$. *Phys. Rev. Lett.* **2011**, *106*, 056404.

(11) Pyykkö, P.; Runeberg, N. Icosahedral WAu_{12}: A Predicted Closed-Shell Species, Stabilized by Aurophilic Attractionand Relativity and in Accord with the 18-Electron Rule. *Angew. Chem., Int. Ed.* **2002**, *41*, 2174–2176.

(12) Zhang, M.; Gu, X. Y.; Zhang, W. L.; Zhao, L. N.; He L. M.; Luo, Y. H. Probing the Magnetic and Structural Properties of the 3d, 4d, 5d Impurities Encapsulated in an Icosahedral Ag_{12} Cage. *Phys. B* **2010**, *405*, 642–648.

(13) Gong, X.; Ju, W.; Li, T.; Feng Z.; Wang, Y. Spin–orbit Splitting and Magnetism of Icosahedral M@Ag_{12} Clusters (M = 3*d* and 4*d* atoms). *J. Cluster Sci.* **2015**, *26*, 759–773.

(14) Pham, H. T.; Cuong, N. T.; Tam, N. M.; Tung, N. T. A Systematic Investigation on $CrCu_n$ Clusters with n = 9–16: Noble Gas and Tunable Magnetic Property. *J. Phys. Chem. A* **2016**, *120*, 7335–7343.

(15) Xiong, H.; Die, D.; Xu, Y. G.; Zheng, B. X.; Fu, Y. C. Probing the Structural, Electronic and Magnetic Properties of Ag_nSc (n = 1–16) Clusters. *Phys. Chem. Chem. Phys.* **2018**, *20*, 15824–15834.

(16) Lai, L.; Die, D.; Zheng, B.-X.; Du, Q. Growth Mechanism and Electronic and Magnetic Properties of Ag_nTi Alloy Clusters. *J. Phys. Chem. Solids* **2021**, 148, 109757.

(17) Blades, W. H.; Reber, A. C.; Khanna, S. N.; López-Sosa, L.; Calaminici, P. Köster, A. M. Evolution of the Spin Magnetic Moments and Atomic Valence of Vanadium in VCu_x^+, VAg_x^+, and VAu_x^+ Clusters (x = 3–14). *J. Phys. Chem. A* **2017**, *121*, 2990–2999.

(18) Medel, V. M.; Reber, A. C.; Chauhan, V.; Sen, P.; Köster, A. M.; Calaminici. P.; Khanna, S. N. Nature of Valence Transition and Spin Moment in Ag_nV^+ Clusters. *J. Am. Chem. Soc.* **2014**, *136*, 8229–8236.

(19) Rodríguez-Kessler, P. L.; Rodríguez-Domínguez, A. R. Structural, Electronic, and Magnetic Properties of Ag_nCo (n = 1–9) Clusters: A First-Principles Study. *Comput. Theor. Chem.* **2015**, *1066*, 55–61.

(20) Marín, P.; Alonso, J. A.; Germán, E.; López, M. J. Nanoalloys of Metals Which Do Not Form Bulk Alloys: The Case of Ag–Co. *J. Phys. Chem. A* **2020**, *124*, 6468–6477.

(21) Neukermans, S.; Janssens, E.; Tanaka, H.; Silverans R. E.; Lievens, P. Element- and Size-Dependent Electron Delocalization in Au_NX^+ Clusters (X = Sc, Ti, V, Cr, Mn, Fe, Co, Ni). *Phys. Rev. Lett.* **2003**, *90*, 033401.

(22) Janssens, E.; Tanaka, H.; Neukermans, S.; Silverans R. E.; Lievens, P. Electron Delocalization in Au_NX_M (X = Sc, Ti, Cr, Fe) Clusters: A Density Functional Theory and Photofragmentation Study, *Phys. Rev. B: Condens. Matter Mater. Phys.* **2004**, *69*, 085402.

(23) Janssens, E.; Neukermans, S.; Nguyen, H. M. T.; Nguyen M. T.; Lievens, P. Quenching of the Magnetic Moment of a Transition Metal Dopant in Silver Clusters. *Phys. Rev. Lett.* **2005**, *94*, 113401.

(24) Janssens, E.; Neukermans, S.; Wang, X.; Veldeman, N.; Silverans, R. E.; Lievens, P. Stability Patterns of Transition Metal Doped Silver Clusters: Dopant- and Size-Dependent Electron Delocalization. *Eur. Phys. J. D* **2005**, *34*, 23–27.

(25) Veldeman, N.; Höltzl, T.; Neukermans, S.; Veszprémi, T.; Nguyen, M. T.; Lievens, P. Experimental Observation and Computational Identification of $Sc@Cu_{16}^+$, a Stable Dopant-Encapsulated Copper Cage. *Phys. Rev. A* **2007**, *76*, 011201.

(26) Höltzl, T.; Veldeman, N.; De Haeck, J.; Veszprémi, T.; Lievens, P.; Nguyen, M. T. Growth Mechanism and Chemical Bonding in Scandium-Doped Copper Clusters: Experimental and Theoretical Study in Concert. *Chem.–Eur. J.* **2009**, *15*, 3970–3982.

(27) Hirsch, K.; Zamudio-Bayer, V.; Langenberg, A.; Niemeyer, M.; Langbehn, B.; Möller, T.; Terasaki, A.; von Issendorff, B.; Lau, J. T. Magnetic Moments of Chromium-Doped Gold Clusters: Anderson Impurity Model in Finite Systems. *Phys. Rev. Lett.* **2015**, *114*, 087202.

(28) Leuchtner, R. E.; Harms, A. C.; Castleman, Jr., A. W. Thermal Metal Cluster Anion Reactions: Behavior of Aluminum Clusters with Oxygen. *J. Chem. Phys.* **1989**, *91*, 2753–2754.

(29) Luo, Z.; Gamboa, G. U.; Smith, J. C.; Reber, A. C.; Reveles, J. U.; Khanna, S. N.; Castleman, Jr., A. W. Spin Accommodation and Reactivity of Silver Clusters with Oxygen: The Enhanced Stability of Ag_{13}^-. *J. Am. Chem. Soc.* **2012**, *134*, 18973–18978.

(30) Luo, Z.; Castleman, Jr., A. W.; Khanna, S. N. Reactivity of Metal Clusters. *Chem. Rev.* **2016**, *116*, 14456–14492.

(31) Ito, T.; Egashira, K.; Tsukiyama, K.; Terasaki, A. Oxidation Processes of Chromium Dimer and Trimer Cations in an Ion Trap. *Chem. Phys. Lett.* **2012**, *538*, 19–23.

(32) Arakawa, M.; Kohara, K.; Ito, T.; Terasaki, A. Size-dependent Reactivity of Aluminum Cluster Cations toward Water Molecules. *Eur. Phys. J. D* **2013**, *67*, 80.

(33) Ito, T.; Naresh Patwari, G.; Arakawa, M.; Terasaki, A. Water-Induced Adsorption of Carbon Monoxide and Oxygen on the Gold Dimer Cation, *J. Phys. Chem. A* **2014**, *118*, 8293–8297.

(34) Arakawa, M.; Kohara, K.; Terasaki, A. Reaction of Aluminum Cluster Cations with a Mixture of O_2 and H_2O Gases: Formation of Hydrated-Alumina Clusters. *J. Phys. Chem. C* **2015**, *119*, 10981−10986.

(35) Arakawa, M.; Yamane, R.; Terasaki, A. Reaction Sites of CO on Size-Selected Silicon Oxide Cluster Anions: A Model Study of Chemistry in the Interstellar Environment. *J. Phys. Chem. A* **2016**, *120*, 139−144.

(36) Arakawa, M.; Omoda, T.; Terasaki, A. Adsorption and Subsequent Reaction of a Water Molecule on Silicate and Silica Cluster Anions. *J. Phys. Chem. C* **2017**, *121*, 10790−10795.

(37) Arakawa, M.; Ando, K.; Fujimoto, S.; Mishra, S.; Naresh Patwari, G.; Terasaki, A. The Role of Electronegativity on the Extent of Nitridation of Group 5 Metals as Revealed

by Reactions of Tantalum Cluster Cations with Ammonia Molecules. *Phys. Chem. Chem. Phys.* **2018**, *20*, 13974–13982.

(38) Ito, T.; Arakawa, M.; Taniguchi, Y.; Terasaki, A. Adsorption Kinetics of Nitrogen Molecules on Size-Selected Silver Cluster Cations. *Z. Phys. Chem.* **2019**, *233*, 759−770.

(39) Arakawa, M.; Horioka, M.; Minamikawa, K.; Kawano, T.; Terasaki, A. Reaction Kinetics of Nitric Oxide on Size-Selected Silver Cluster Cations. *J. Phys. Chem. C* **2020**, *124*, 26881−26888.

(40) Arakawa, M.; Okada, D.; Kono, S.; Terasaki, A. Preadsorption Effect of Carbon Monoxide on Reactivity of Cobalt Cluster Cations toward Hydrogen. *J. Phys. Chem. A* **2020**, *124*, 9751−9756.

(41) Arakawa, M.; Horioka, M.; Minamikawa, K.; Kawano, T.; Terasaki, A. Reaction of Nitric Oxide Molecules on Transition-Metal-Doped Silver Cluster Cations: Size- and Dopant-Dependent Reaction Pathways. *Phys. Chem. Chem. Phys.* **2021**, *23*, 22947−22956.

(42) Sarugaku, S.; Murakami, R.; Matsumoto, J.; Kawano, T.; Arakawa, M.; Terasaki, A. Size-Dependent Reactivity of Nickel-Doped Silver Cluster Cations toward Oxygen: Electronic and Geometric Effect. *Chem. Lett.* **2017**, *46*, 385−388.

(43) Sarugaku, S.; Arakawa, M.; Kawano, T.; Terasaki, A. Electronic and Geometric Effects on Chemical Reactivity of 3d-Transition-Metal-Doped Silver Cluster Cations toward Oxygen Molecules. *J. Phys. Chem. C* **2019**, *123*, 25890−25897.

(44) Minamikawa, K.; Arakawa, M.; Tono, K.; Terasaki, A. A Revisit to Electronic Structures of Cobalt-Doped Silver Cluster Anions by Size-Dependent Reactivity Measurement. *Chem. Phys. Lett.* **2020**, *753*, 137613.

(45) Minamikawa, K.; Sarugaku, S.; Arakawa, M.; Terasaki, A. Electron Counting in Cationic and Anionic Silver Clusters Doped with a 3d Transition-Metal Atom: Endo- vs. Exohedral Geometry. *Phys. Chem. Chem. Phys.* **2022**, *24*, 1447−1455.

(46) Haberland, H.; Karrais, M.; Mall, M.; Thurner, Y. Thin Films from Energetic Cluster Impact: A Feasibility Study, *J. Vac. Sci. Technol. A* **1992**, *10*, 3266.

(47) Guo, B. C.; Kerns, K. P.; Castleman, A. W., Jr. Chemistry and Kinetics of Size-Selected Cobalt Cluster Cations at Thermal Energies. 2. Reactions with Oxygen. *J. Phys. Chem.* **1992**, *96*, 6931–6937.

(48) Sarugaku, S.; Arakawa, M.; Terasaki, A. Space Focusing Extensively Spread Ions in Time-of-Flight Mass Spectrometry by Nonlinear Ion Acceleration, *Int. J. Mass Spectrom.* **2017**, *414*, 65–69.

(49) Handa, T.; Horio, T.; Arakawa, M.; Terasaki, A. Improvement of Reflectron Time-of-Flight Mass Spectrometer for Better Convergence of Ion Beam, *Int. J. Mass Spectrom.* **2020**, *451*, 116311.

(50) Koyanagi, G. K.; Bohme, D. K. Oxidation Reactions of Lanthanide Cations with N_2O and O_2: Periodicities in Reactivity. *J. Phys. Chem. A* **2001**, *105*, 8964−8968.

(51) Jackschath, C.; Rabin, I.; Schulze, W. Electron impact ionization of silver clusters Ag., $n \leq 36$. *Z. Phys. D: At., Mol. Clusters.* **1992**, *22*, 517−520.

(52) Levin, N.; Margraf, J. T.; Lengyel, J.; Reuter, K.; Tschurl, M.; Heiz, U. CO_2-Activation by Size-Selected Tantalum Cluster Cations ($Ta_{1–16}^+$): Thermalization Governing Reaction Selectivity. *Phys. Chem. Chem. Phys.* **2022**, *24*, 2623–2629.

(53) Koyasu, K.; Atobe, J.; Akutsu, M.; Mitsui, M.; Nakajima, A. Electronic and Geometric Stabilities of Clusters with Transition Metal Encapsulated by Silicon. *J. Phys. Chem. A* **2007**, *111*, 42–49.

(54) Zamudio-Bayer, V.; Leppert, L.; Hirsch, K.; Langenberg, A.; Rittmann, J.; Kossick, M.; Vogel, M.; Richter, R.; Terasaki, A.; Möller T. et al. Coordination-Driven Magnetic-to-Nonmagnetic Transition in Manganese-Doped Silicon Clusters. *Phys. Rev. B: Condens. Matter Mater. Phys.* **2013**, *88*, 115425.

(55) Hirabayashi, S.; Ichihashi, M. Reactions of Ti- and V-Doped Cu Cluster Cations with Nitric Oxide and Oxygen: Size Dependence and Preferential NO Adsorption. *J. Phys. Chem. A* **2016**, *120*, 1637–1643.

(56) Schumacher, E. *DETMECH − Chemical Reaction Kinetics Software*, University of Bern, Bern, Switzerland, 2003.

Table of Content Artwork